Supporting Information: Observation of a Rare Earth Ion-Extractant Complex Arrested at the Oil-Water Interface During Solvent Extraction

Wei Bu,[,1] Hao Yu,[1] Guangming Luo,[2] Mrinal K. Bera,[1] Binyang Hou,[1] Adam W. Schuman,[1] Binhua Lin,[3] Mati Meron,[3] Ivan Kuzmenko,[4] Mark R. Antonio,[2] L. Soderholm,[*,2] Mark L. Schlossman[*,1]*

[1]Department of Physics, University of Illinois at Chicago, Chicago, IL 60607, USA.
[2]Chemical Sciences and Engineering Division, Argonne National Laboratory, Argonne, IL 60439, USA.
[3]Center for Advanced Radiation Sources, University of Chicago, Chicago, IL 60637, USA.
[4]XSD, Advanced Photon Source, Argonne National Laboratory, Argonne, IL 60439, USA.

S1. X-ray Fluorescence near Total Reflection (XFNTR) Reference Sample

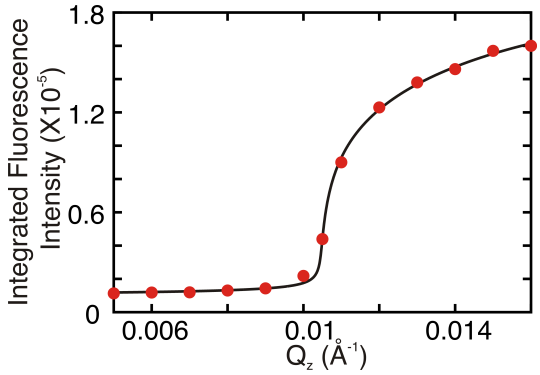

Figure S1. The integrated fluorescence intensity of Er $L\alpha$ emission lines from a reference sample (i.e., the interface between pure dodecane and a 0.1 M aqueous solution of $ErBr_3$) is shown as a function of wave vector transfer Q_z. The solid line is the best fit that determines the scale factor $C = 7.48\times10^{-7}$ Å. Error bars are smaller than the symbols.

S2. Area per Molecule Calculation for Sample without Erbium

To determine the area per DHDP molecule for the sample without erbium, we set the arbitrary position $z = 0$ to be at the center of C-O bond and assume that dodecane molecules to not intercalate into the monolayer. Subsequently, the area per molecule A can be calculated as

$$A = \frac{258}{d_2\rho_2 + d_3\rho_3}, \qquad [S1]$$

where the total number of electrons in the two alkyl chains ($2\times[CH_3(CH_2)_{15}]$) of a DHDP molecule is 258. Substituting the best-fit parameters from the first row in Table 1 (28 °C) into Eq. [S1] yields the molecular area $42.7^{+2.2}_{-1.9}$ Å^2.

For the sample without erbium at 50 °C (above the transition), the volume and total number of electrons in the first layer are expressed as

$$d_1 A = N_{H_2O} V_{H_2O} + V_{PO_4^-}$$
$$\rho_1 d_1 A = N_{H_2O} Z_{H_2O} + Z_{PO_4^-}, \qquad [S2]$$

where N, V, and Z represent the number, volume, and total number of electrons for each species, respectively. Using the constants $Z_{H_2O} = 10$, $V_{H_2O} = 30$ Å^3, and $Z_{PO_4^-} = 48$, the volume of the headgroup $V_{PO_4^-} = 62^{+4}_{-4}$ Å^3 is calculated from the fitting parameters in Table 1 and $A = 42.7^{+2.2}_{-1.9}$ Å^2 calculated above for the data at 28 °C. Substituting these constants, as well as the fitting parameters in the second row of Table 1 for the 50 °C data, into Eq. S2 yields the molecular area 82^{+11}_{-7} Å^2 for sample at 50 °C, consistent with a calculation using Eq. S1 and the tail parameters for the 50 °C data, which yields 78^{+10}_{-6} Å^2. Calculations from Eq. [S2] also yield the number of water molecules in the head group region: $N_{H_2O} = 4$ at 28 °C and $N_{H_2O} = 8$ at 50 °C.

Eq. S2 was also used to estimate the maximum coverage of DHDP molecules that have their head groups in contact with the aqueous phase (referred to as DHDP anchors in the main text), see Fig. 5C. Eq. S1 cannot be used for this calculation because the head groups of most DHDP in the lower leaflet are located in the middle region of the inverted bilayer. An additional thin slab, associated with the headgroup of DHDP anchors, was inserted between the aqueous phase and the lower leaflet to model X-ray reflectivity data. Fitting parameters from this thin slab, combined with Eq. S2, yield the minimum molecular area of DHDP anchors to be ~ 450 Å^2, i.e., ~10% of the interfacial area.

S3. High Temperature X-ray reflectivity Data

Figure S2 illustrates X-ray reflectivity $R(Q_z)/R_F(Q_z)$ at 50 °C from the interface between pure water and 10^{-4} M DHDP in dodecane and from an interface between 10^{-4} M DHDP in dodecane and 5 x 10^{-7} M $ErBr_3$ in water (*p*H=2.5 adjusted with HBr). These data are greatly reduced in amplitude and represent an interface with a much lower density of DHDP. Nevertheless, the presence of a weak peak indicates that the DHDP density has not been reduced to zero. This is consistent with the reduction of interfacial tension below that of the pure water/dodecane interface at 50 °C illustrated in Fig. 1.

The lines in this figure demonstrate that these data cannot be fit by assuming that the transition T_0 is just a chain-disordering transition, *i.e.*, the DHDP molecules fully cover the interface with a monolayer below and above T_0, but the chains disorder (all-trans to some gauche conformations along the chain) upon heating through T_0. Note that even if the disordered chains had exactly the same electron density as dodecane, the headgroups of DHDP are still present and will reflect X-rays. In this case, the X-ray reflectivity would record a peak at higher Q_z that corresponds to this thin layer of headgroups, whereas the data show a weak peak at lower Q_z. The lines in Fig. S2 illustrate this effect. The solid line corresponds to modeling the melted chains with an electron density of 0.265 e$^-$Å^{-3}, similar to previous observations of melted chains

at the water/hexane interface [1]. The dashed line corresponds to perfect matching of X-ray contrast between the DHDP chains and dodecane. In both cases, the presence of the DHDP headgroup produces peaks at higher Q_z that are not observed in the data.

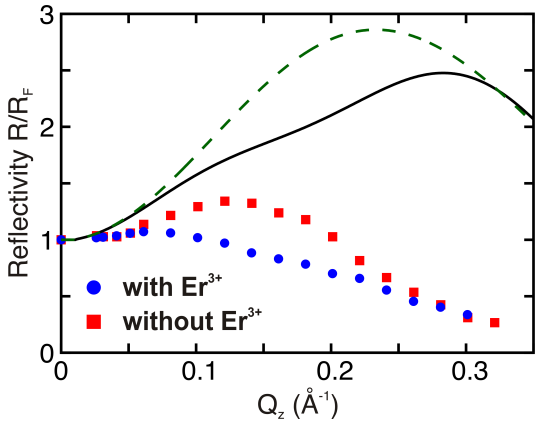

Figure S2. Normalized X-ray reflectivity $R(Q_z)/R_F(Q_z)$ from the interface at 50 °C between 10^{-4} M DHDP in dodecane and pure water (solid red squares) and an interface between 10^{-4} M DHDP in dodecane and 10^{-7} M $ErBr_3$ in water (*p*H=2.5 adjusted with HBr; blue dots). The lines are simulated X-ray reflectivity discussed in the text, which demonstrate that these data cannot be fit by assuming that the transition at T_0 is a chain-melting transition.

S4. Low Q_z X-ray reflectivity Data Analysis

The low Q_z feature of the X-ray reflectivity shown in Fig. 5 can be understood qualitatively by an approximate analysis that utilizes the Born approximation for x-ray scattering which relates the reflectivity to the electron density gradient normal to the interface,[2]

$$\frac{R(Q_z)}{R_F(Q_z)} = \left| \frac{1}{\rho_0 - \rho_N} \int \frac{d\rho(z)}{dz} \exp(-iQ_z z) dz \right|^2 . \qquad [S3]$$

Substituting Eq. 1 from the main text,

$$\rho(z) = \frac{1}{2} \sum_{i=0}^{N-1} \mathrm{erf}\left(\frac{z - z_i}{\sqrt{2}\sigma} \right) (\rho_i - \rho_{i+1}) + \frac{\rho_0 + \rho_N}{2}$$

into Eq. S3 yields

$$\frac{R(Q_z)}{R_F(Q_z)} = \left| \frac{1}{\rho_0 - \rho_N} \frac{1}{2} \sum_{i=0}^{N-1} (\rho_i - \rho_{i+1}) \int \frac{d}{dz} \left(\mathrm{erf}\left(\frac{z - z_i}{\sqrt{2}\sigma} \right) \right) \exp(-iQ_z z) dz \right|^2$$

$$= \left| \frac{1}{\rho_0 - \rho_N} \frac{1}{\sqrt{2\pi}\sigma} \sum_{i=0}^{N-1} (\rho_i - \rho_{i+1}) \int e^{-\left(\frac{z-z_i}{\sqrt{2}\sigma}\right)^2} e^{-iQ_z z} dz \right|^2$$

$$= \left| \frac{1}{\rho_0 - \rho_N} \frac{1}{\sqrt{2\pi}\sigma} \sum_{i=0}^{N-1} (\rho_i - \rho_{i+1}) \sqrt{2\pi}\sigma e^{-Q_z^2\sigma^2/2} e^{-iQ_z z_i} \right|^2$$

$$= \frac{e^{-Q_z^2\sigma^2}}{(\rho_0 - \rho_N)^2} \left| \sum_{i=0}^{N-1} (\rho_i - \rho_{i+1}) e^{-iQ_z z_i} \right|^2$$

$$= \frac{e^{-Q_z^2\sigma^2}}{(\rho_0 - \rho_N)^2} \left(\sum_{i=0}^{N-1} (\rho_i - \rho_{i+1})^2 + 2 \sum_{i=0}^{N-1} \sum_{j>i}^{N-1} (\rho_i - \rho_{i+1})(\rho_j - \rho_{j+1}) \cos(Q_z (z_i - z_j)) \right). \quad \text{[S4]}$$

Equation S4 consists of a Gaussian term that multiplies Q_z-independent and Q_z-dependent terms from each internal interface. At low Q_z, under conditions where the electron density contrast is greatest at the top and bottom of the interfacial layer, the dominant Q_z-dependent term is due to the internal interfaces at the top and bottom of the layer, with $R/R_F \propto (\rho_0 - \rho_1)(\rho_{N-1} - \rho_N)\cos(Q_z d)$, where $d = |z_0 - z_{N-1}|$ is the total internal thickness. Therefore, the qualitative behavior of the reflectivity at low Q_z depends upon the relative signs of $\rho_0 - \rho_1$ and $\rho_{N-1} - \rho_N$. For example, in the case of a monolayer described by 2 slabs, these two terms have opposite signs. This leads to a $-\cos(Q_z d)$ behavior so that R/R_F rises above 1 at low Q_z. The monolayer profile in Fig. 3C actually has a third slab with a very weak electron density contrast, so that the argument has to consider $\rho_0 - \rho_1$ and $\rho_{N-2} - \rho_{N-1}$ (because $\rho_{N-2} - \rho_{N-1} \gg \rho_{N-1} - \rho_N$). The opposite is true for the inverted bilayer, for which these two terms, $\rho_0 - \rho_1$ and $\rho_{N-1} - \rho_N$, have the same sign (see Fig. 5B). This leads to a $+\cos(Q_z d)$ behavior and a decrease in R/R_F below 1 at low Q_z.

S5. X-ray Fluorescence near Total Reflection (XFNTR) Br^- Coverage

XFNTR was used to determine the Br^- coverage at the interface between a 10^{-4} M dodecane solution of DHDP and a 5×10^{-7} M aqueous solution of $ErBr_3$.[3] The integrated fluorescence intensity of Br $K\alpha$ emission lines (Fig. S3A) measured for values of Q_z near Q_c is illustrated in Fig. S3B. The overall shape is similar to the measurement from the reference sample, implying that the bulk contribution from $10^{-2.5}$ M HBr dominates the signal. The transition at Q_c appears rounded, as a result of the interfacial radius of curvature of 90±7 m. The fit determined that a negligible amount of Br^- is at the interface: one Br^- per 1300 $Å^2$ (with an upper limit of one Br^- per 500 $Å^2$ or 370 $Å^2$ at the 95% confidence level). Also shown in Fig. S3B,C is a dashed line that illustrates the predicted fluorescence if Br^- ions have the same interfacial area per ion as the Er^{3+} (81$Å^2$), which demonstrates that this prediction for a higher density Br^- at the interface is inconsistent with the data below Q_c.

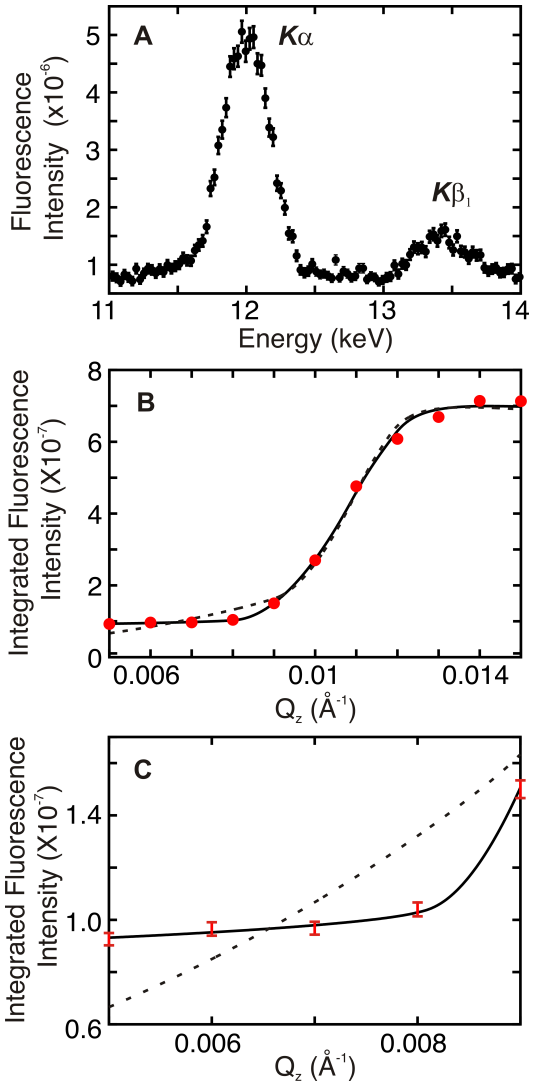

Figure S3. X-ray fluorescence data and analysis. X-ray fluorescence spectra of Br (A) measured below the critical angle at $Q_z = 0.008$ Å^{-1} (X-ray penetration depth of 170 Å) from the interface between 10^{-4} M DHDP in dodecane and 5×10^{-7} M $ErBr_3$ in water (*p*H=2.5, adjusted with HBr) at 28°C. Intensity is dominated by the interfacial (I_I) and background signal (I_b) for Er and Br, respectively. (B) The integrated fluorescence intensity from Br $K\alpha$ emission lines shown in (B). The solid line is the best fit, yielding the interfacial radius of curvature of 90±7 m and one Br^- per 1300 Å^2. The dashed line illustrates the best fit with the area per Br^- fixed at 81 Å^2 in order to demonstrate the variation with Br^- interfacial density. (C) Expanded view of lower Q_z region of panel C, which shows the error bars.

S6. Alternate Inverted Bilayer Structure with Higher Density Lower Leaflet

Figure S4 and Table S1 illustrate the fit to the alternate inverted bilayer discussed in the main text near Fig. 12. The lower leaflet of this alternate inverted bilayer is higher density than

the bilayer shown in Fig. 5. The reflectivity data appear quite different. The higher frequency oscillations in the reflectivity data in Fig. 5 are absent from Fig. S4A because of the near match in electron density between the aqueous phase and the lower leaflet ρ_1. The characteristic signature of an inverted bilayer still appears at low Q_z in Fig. S4A, but greatly damped because of the near match in electron density just mentioned. Here, it appears as a relatively flat variation in $R(Q_z)/R_F(Q_z)$ at low Q_z, still distinguishable from the rise in intensity expected for monolayers, regular bilayers, and trilayers. The structures in Fig. S4 and in Fig. 5 were each measured on multiple samples.

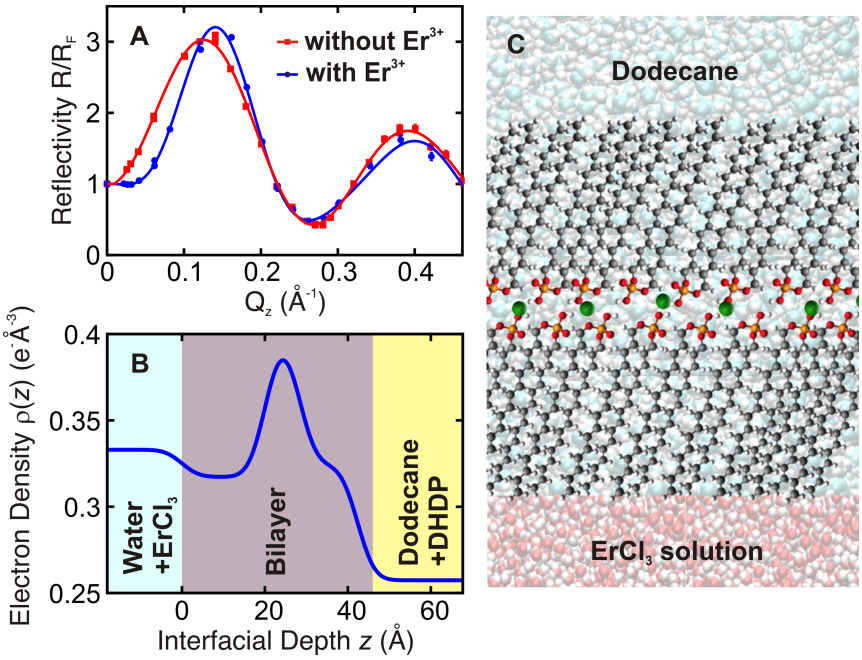

Figure S4. X-ray reflectivity results for the alternate form of the inverted bilayer (A) Normalized X-ray reflectivity $R(Q_z)/R_F(Q_z)$ from the interface between 10^{-7} M $ErCl_3$ in water (*p*H=2.5 adjusted with HCl) and 10^{-4} M DHDP in dodecane (dots with blue line fit), and for comparison (also shown in Fig. 3), from the interface between pure water and 10^{-4} M DHDP in dodecane (squares with red line fit), both at 28 °C. Points at $Q_z = 0$ are measured from transmission through the bulk organic phase. The blue line is the best fit calculated from the electron density profile shown in (B), which provides the basis for the inverted bilayer with $ErCl_3$ illustrated in (C).

Table S1. Best-fit parameters to the X-ray reflectivity data[a]

#	σ	d_1	ρ_1	d_2	ρ_2	d_3	ρ_3	d_3	ρ_3
layers	(Å)	(Å)	($e^-/Å^3$)	(Å)	($e^-/Å^3$)	(Å)	($e^-/Å^3$)	(Å)	($e^-/Å^3$)
three	$3.3^{+0.3}_{-0.3}$	$20.2^{+0.4}_{-1.3}$	$0.317^{+0.001}_{-0.001}$	$8.1^{+1.7}_{-2.1}$	$0.402^{+0.025}_{-0.012}$	$14.1^{+1.1}_{-0.9}$	$0.324^{+0.005}_{-0.005}$		
four	$3.4^{+0.3}_{-0.4}$	$20.6^{+0.0}_{-1.3}$	$0.318^{+0.001}_{-0.001}$	$8.5^{+1.5}_{-2.4}$	$0.401^{+0.015}_{-0.011}$	$14.4^{+1.5}_{-0.8}$	$0.319^{+0.006}_{-0.003}$	$5.5^{+0.5}_{-2.5}$	$0.249^{+0.005}_{-0.029}$

[a] Fits to data from interfaces between 10^{-4} M DHDP in dodecane and 10^{-7} M $ErCl_3$ in water (*p*H=2.5, adjusted with HCl) at 28 °C. The electron densities of the bulk aqueous and organic phases are 0.333 $e^-/Å^3$ and 0.2574 $e^-/Å^3$, respectively, at 28 °C. Three layer fit is shown in Fig. S4; the four layer fit is slightly better at the highest values of Q_z.

SI References

(1) Tikhonov, A. M.; Pingali, S. V.; Schlossman, M. L. Molecular ordering and phase transitions in alkanol monolayers at the water-hexane interface. *J. Chem. Phys.* **2004**, *120*, 11822-11838.

(2) Pershan, P. S.; Schlossman, M. L. *Liquid Surfaces and Interfaces: Synchrotron X-ray Methods*; Cambridge University Press: Cambridge, 2012.

(3) Bu, W.; Hou, B.; Mihaylov, M.; Kuzmenko, I.; Lin, B.; Meron, M.; Soderholm, L.; Luo, G.; Schlossman, M. L. X-ray fluorescence from a model liquid/liquid solvent extraction system. *J. Appl. Phys.* **2011**, *110*, 102214.